

A 3-D Near-Field Modeling Approach for Electromagnetic Interference Prediction

Hanan Shall, *Student Member, IEEE*, Zouheir Riah, and Moncef Kadi

Abstract—This paper presents, through an illustrative example, a 3-D modeling approach to predict the electromagnetic interference (EMI) between complex electronic devices and interconnections placed in the near-field region. Three different analytic coupling formulations have been investigated along with a 3-D-emission model to evaluate the induced voltages in transmission line (TL) extremities in the case of both matched and mismatched TL configurations. The proposed modeling method is successfully validated by comparison with numerical results using electromagnetic (EM) simulation tools and experimental results using near-field measurement. The obtained EM coupling results are more accurate than other traditional 2-D models.

Index Terms—Analytic coupling formulations, near-field measurement, transmission lines (TL), 3-D-emission model.

I. INTRODUCTION

IN the last few decades, a large number of complex electronic devices have been incorporated into embedded electronic boards in vehicles in order to improve their performances as in the case of hybrid/electric models. However, this cohabitation can lead to more severe constraints in terms of quality, reliability, and safety due to the increase of EMI between the different components. Therefore, the big challenge of automobile manufacturers is to ensure a good level of competitiveness of their products in a very harsh operating environment. To achieve this target, it becomes necessary to decrease the EM emissions from sources that can be controlled, and/or to increase the immunity of devices that could be affected by such disturbances in radiated or conducted modes.

In order to overcome difficulties related to tighter system integration, automobile designers are sharpening their efforts to guarantee a whole system optimization against electromagnetic compatibility (EMC) problems directly from the first system design steps. For this purpose and to meet their needs, different EMC modeling approaches have been proposed in the literature to predict the level of devices radiated emission. Some of the

proposed models require the knowledge of both internal function and architecture of the device under test (DUT) in order to identify equivalent sources which radiate the same field as the DUT [1]. Other models are generic [2]–[8] (i.e., they do not require any DUT functional specifications) so they offer a better preservation of confidentiality for designers. The work presented in [5] shows efficiency to reproduce the magnetic field using two different approaches: a set of electric dipoles or a set of magnetic dipoles. Two subsequent modeling approaches have been derived: the process described in [6] is based on a set of both electric and magnetic dipoles, whereas the model reported in [7] evaluates the EM radiated fields through the use of only electric sources but taking into consideration the effect of the effective relative permittivity ϵ_{reff} of the medium surrounding the DUT. An improved dipole-moment model was proposed in [8]. Regularization technique and the truncated singular-value decomposition (SVD) method are used to ensure accuracy in near-field prediction. The derived dipole moments model gives information about voltage and current distributions in integrated circuits (ICs).

The previously cited approaches provide models called 2-D models regardless of the DUT geometry. In fact, all the elemental sources are well distributed in the XY plane and radiate the same field as the DUT at higher planes. The computed fields can be used to predict the EM crosstalk between DUTs and other associated interconnections placed in its vicinity. In [9] and [10], authors present an analysis of radiated EM disturbances between devices, represented by their 2-D emission model, considering an approximated solution which is only valid for the case of matched TL [11].

The prediction of such interferences becomes complex when DUT presents a 3-D geometry and it becomes more complex when structures under test have very diverse form factors as the case of power electronics. In this situation, it is necessary to consider the radiation on the different DUT sides. The work reported in [12] presents the first results of a 3-D modeling approach able to compute the EM field in the DUT surrounding space. The 3-D modeling process is mainly inspired from the work presented in [6] and it has been improved to take into account the 3-D radiated fields.

In this paper, we present a 3-D near-field modeling approach offering more accuracy in terms of EMI prediction. The proposed model combines the 3-D emission model explained in [12] with three analytic coupling formulations: Taylor [13], Agrawal [14], and Rachidi [15] to evaluate the induced voltages in TL extremities placed above the DUT. This latter is a simple 3-D structure: a small “arch” above a ground plane used as an illustrative example to validate the proposed model. The contribution

Manuscript received January 21, 2013; revised April 30, 2013; accepted July 13, 2013. Date of publication August 7, 2013; date of current version January 27, 2014. This work was supported by the French government via the ANR under the framework of the E-CEM project.

H. Shall is with Research Institute for Embedded Systems, Saint Etienne du Rouvray 76801, France, and also with the University of Rouen, Mont Saint Aignan 76821, France (e-mail: hanan.shall@esigelec.fr).

Z. Riah and M. Kadi are with the Research Institute for Embedded Systems, Saint Etienne du Rouvray 76801, France (e-mail: riah@esigelec.fr; kadi@esigelec.fr).

Color versions of one or more of the figures in this paper are available online at <http://ieeexplore.ieee.org>.

Digital Object Identifier 10.1109/TEMC.2013.2274576

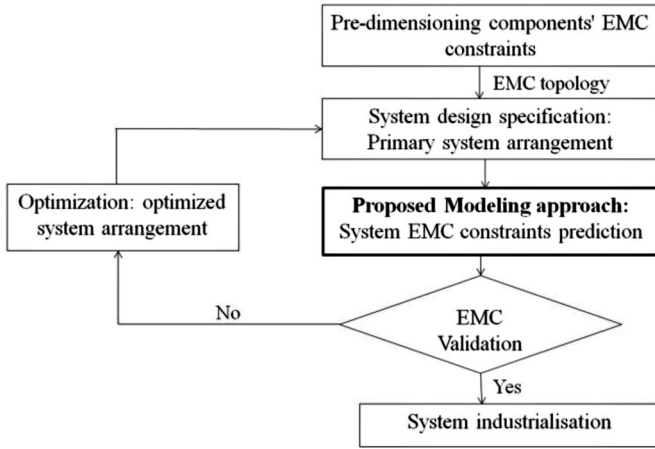


Fig. 1. Optimized design process.

of the proposed modeling approach is very relevant in the system design process (see Fig. 1). In fact, it enables us to predict EMC constraints for components, and consequently for the whole system. Modeling results give designers clearer ideas to optimize system component arrangement in order to reduce hazardous EMC problems.

In the first part of this paper, the 3-D emission model is presented. The cartographies of near-field components used to build up the model are extracted from high frequency simulator structure (HFSS)-Ansys tool [16]. The model is built considering a lower number of dipoles. A 3-D magnetic near-field measurement, using the near-field test bench developed within the Research Institute for Electronic Embedded Systems (IRSEEM) [17], has been carried out to validate modeled results. In the second part, the 3-D near-field coupling model is explained. The obtained results highlight the benefit of the proposed approach compared to other existing models. In fact, they show a more precise coupling prediction between components and interconnections.

II. PRESENTATION OF THE 3-D EMISSION MODEL

A. Principle of the Model

In this approach, at a given frequency, the DUT is replaced by a set of electric and magnetic dipoles distributed on the five surfaces of a parallelepiped surrounding the DUT as shown in Fig. 2. At each considered point, both electric and magnetic dipoles are placed. The sixth face is not taken into account since it is situated under the electronic board ground plane.

Each dipole is defined by specific parameters: dipole length l_e, l_m , current through it I_e, I_m , center position $\{(x_{0e}, y_{0e}, z_{0e}), (x_{0m}, y_{0m}, z_{0m})\}$, azimuth orientation Φ_e, Φ_m , and orientation with respect to z -axis (θ_e, θ_m) , respectively, for electric and magnetic dipoles. To simplify the modeling approach, some of these parameters are prefixed by the user: length, position of each dipole, and the operating frequency f . The distances, corresponding to each considered surface, $(R_{XYi}, R_{YZ3i}, \dots)$

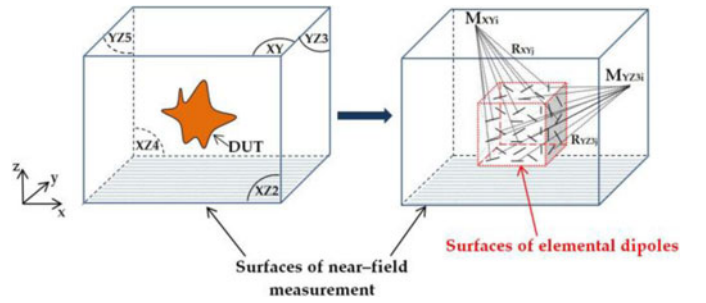


Fig. 2. Principle of the 3-D model.

between dipoles and observation points $(M_{XYi}, M_{YZ3}, \dots)$ are also predefined (see Fig. 2). However, the orientation $\{(\Phi_e, \theta_e), (\Phi_m, \theta_m)\}$ and the currents I_e, I_m are the unknown parameters to be determined. For simplicity reasons, the sources current is assumed to have constant value along l_e and l_m because dipole length is taken very less than λ (1-mm length $\ll \lambda$), λ is the wavelength.

To build up the model, tangential cartographies of EM fields on the different surfaces of a well-defined volume surrounding the DUT and having the following coordinates $\{(x_{\min}, x_{\max}), (y_{\min}, y_{\max}), (z_{\min}, z_{\max})\}$ are used as input data (see Fig. 2). Consequently, five planes are defined and associated tangential components are cited as follows:

- 1) XY plane, where $z = z_{\max}$: $H_{x1}, H_{y1}, E_{x1}, E_{y1}$
- 2) XZ₂ plane, where $y = y_{\min}$: $H_{x2}, H_{z2}, E_{x2}, E_{z2}$
- 3) YZ₃ plane, where $x = x_{\max}$: $H_{y3}, H_{z3}, E_{y3}, E_{z3}$
- 4) XZ₄ plane, where $y = y_{\max}$: $H_{x4}, H_{z4}, E_{x4}, E_{z4}$
- 5) YZ₅ plane, where $x = x_{\min}$: $H_{y5}, H_{z5}, E_{y5}, E_{z5}$

For each measurement point M_i and depending on the considered surface, four tangential EM field components should be known to construct the model.

B. Extraction Process

Mathematical formulation of the model is derived from the electric and magnetic dipoles EM radiation expressions at a given point $M_i(x, y, z)$. They are established from magnetic vector potential \vec{A} and electric vector potential \vec{F} [18]. The mathematical description can be resumed to a matrix system describing an inverse problem $([E, H]_{r \times 1} = [\alpha]_{r \times s} [X]_{s \times 1})$ in (1), as shown at the bottom of the next page, where $r/4$ are the number of points where fields are measured, the matrix elements α_{ij} are constants depending on the pre-fixed parameters (frequency, length, position of dipoles), and $s/2$ is equal to the dipoles number.

To get the orientations and the currents through dipoles, we have to solve the inverse problem described in (1). The elements of the $[E, H]$ matrix and their associated rows in the $[\alpha]$ matrix are normalized to get a well-conditioned inverse problem [6]. A least-square inversion method is applied to get the $[X]$ matrix, i.e., to obtain the vectors $[AE_j], [BE_j], [AH_j],$ and $[BH_j]$

presented in (2), where $j = \{XY, XZ_2, YZ_3, XZ_4, YZ_5\}$

$$[E, H]_{s \times 1} [\alpha]_{r \times s}^{-1} = \begin{bmatrix} \begin{bmatrix} AE_{XY} \\ BE_{XY} \end{bmatrix}_{XY} \\ \begin{bmatrix} AE_{XZ_2} \\ BE_{XZ_2} \end{bmatrix}_{XZ_2} \\ \begin{bmatrix} AE_{YZ_3} \\ BE_{YZ_3} \end{bmatrix}_{YZ_3} \\ \begin{bmatrix} AE_{XZ_4} \\ BE_{XZ_4} \end{bmatrix}_{XZ_4} \\ \begin{bmatrix} AE_{YZ_5} \\ BE_{YZ_5} \end{bmatrix}_{YZ_5} \\ \begin{bmatrix} AH_{XY} \\ BH_{XY} \end{bmatrix}_{XY} \\ \begin{bmatrix} AH_{XZ_2} \\ BH_{XZ_2} \end{bmatrix}_{XZ_2} \\ \begin{bmatrix} AH_{YZ_3} \\ BH_{YZ_3} \end{bmatrix}_{YZ_3} \\ \begin{bmatrix} AH_{XZ_4} \\ BH_{XZ_4} \end{bmatrix}_{XZ_4} \\ \begin{bmatrix} AH_{YZ_5} \\ BH_{YZ_5} \end{bmatrix}_{YZ_5} \end{bmatrix}_{s \times 1}$$

The orientations can then be evaluated by a division element-by-element inside the $[X]$ matrix [see (3)]

$$\theta_{ei} = \arctan\left(\frac{AE_j}{BE_j}\right); \theta_{mi} = \arctan\left(\frac{AH_j}{BH_j}\right) \quad (3)$$

where i corresponds to each elemental source. Once the orientations of dipoles are determined, a matrix $[\beta]_{r \times (s/2)}$, containing the orientations already computed and the predefined parameters, can be illustrated in the following equation:

$$(2) \quad [E, H]_{r \times 1} = \begin{pmatrix} \beta_{1,1} & \cdots & \beta_{1,s/2} \\ \vdots & \ddots & \vdots \\ \beta_{r,1} & \cdots & \beta_{r,s/2} \end{pmatrix}_{r \times (s/2)} \begin{pmatrix} [I_e]_{XY} \\ [I_e]_{XZ_2} \\ [I_e]_{YZ_3} \\ [I_e]_{XZ_4} \\ [I_e]_{YZ_5} \\ [I_m]_{XY} \\ [I_m]_{XZ_2} \\ [I_m]_{YZ_3} \\ [I_m]_{XZ_4} \\ [I_m]_{YZ_5} \end{pmatrix}_{(s/2) \times 1}$$

$$= [\beta]_{r \times (s/2)} [I_e, I_m]_{(s/2) \times 1} \quad (4)$$

The same inversion method is carried out to get the currents flowing through dipoles: $[I_e, I_m]_{(s/2) \times 1} = [\beta]_{r \times (s/2)}^{-1} [E, H]_{r \times 1}$.

$$\begin{bmatrix} \begin{bmatrix} H_x \\ H_y \end{bmatrix}_{XY} \\ \begin{bmatrix} H_{x2} \\ H_{z2} \end{bmatrix}_{XZ_2} \\ \begin{bmatrix} H_{y3} \\ H_{z3} \end{bmatrix}_{YZ_3} \\ \begin{bmatrix} H_{x4} \\ H_{z4} \end{bmatrix}_{XZ_4} \\ \begin{bmatrix} H_{y5} \\ H_{z5} \end{bmatrix}_{YZ_5} \\ \begin{bmatrix} E_x \\ E_y \end{bmatrix}_{XY} \\ \begin{bmatrix} E_{x2} \\ E_{z2} \end{bmatrix}_{XZ_2} \\ \begin{bmatrix} E_{y3} \\ E_{z3} \end{bmatrix}_{YZ_3} \\ \begin{bmatrix} E_{x4} \\ E_{z4} \end{bmatrix}_{XZ_4} \\ \begin{bmatrix} E_{y5} \\ E_{z5} \end{bmatrix}_{YZ_5} \end{bmatrix}_{r \times 1} = \begin{pmatrix} \alpha_{1,1} & \cdots & \alpha_{1,s} \\ \vdots & \ddots & \vdots \\ \alpha_{r,1} & \cdots & \alpha_{r,s} \end{pmatrix}_{r \times s} \begin{bmatrix} \begin{bmatrix} I_e \sin \theta_e \sin \phi_e \\ I_e \sin \theta_e \cos \phi_e \end{bmatrix}_{XY, \theta_e = \pi/2} \\ \begin{bmatrix} I_e \sin \theta_e \cos \phi_e \\ I_e \cos \theta_e \end{bmatrix}_{XZ_2, \phi_e = 0} \\ \begin{bmatrix} I_e \sin \theta_e \sin \phi_e \\ I_e \cos \theta_e \end{bmatrix}_{YZ_3, \phi_e = \pi/2} \\ \begin{bmatrix} I_e \sin \theta_e \cos \phi_e \\ I_e \cos \theta_e \end{bmatrix}_{XZ_4, \phi_e = 0} \\ \begin{bmatrix} I_e \sin \theta_e \sin \phi_e \\ I_e \cos \theta_e \end{bmatrix}_{YZ_5, \phi_e = \pi/2} \\ \begin{bmatrix} I_m \sin \theta_m \sin \phi_m \\ I_m \sin \theta_m \cos \phi_m \end{bmatrix}_{XY, \theta_m = \pi/2} \\ \begin{bmatrix} I_m \sin \theta_m \cos \phi_m \\ I_m \cos \theta_m \end{bmatrix}_{XZ_2, \phi_m = 0} \\ \begin{bmatrix} I_m \sin \theta_m \sin \phi_m \\ I_m \cos \theta_m \end{bmatrix}_{YZ_3, \phi_m = \pi/2} \\ \begin{bmatrix} I_m \sin \theta_m \cos \phi_m \\ I_m \cos \theta_m \end{bmatrix}_{XZ_4, \phi_m = 0} \\ \begin{bmatrix} I_m \sin \theta_m \sin \phi_m \\ I_m \cos \theta_m \end{bmatrix}_{YZ_5, \phi_m = \pi/2} \end{bmatrix}_{s \times 1} \quad (1)$$

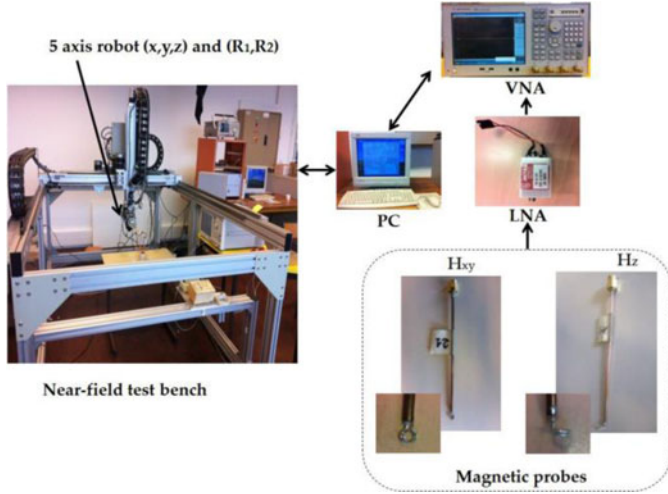


Fig. 3. Near Field test bench setup, different measurement equipment and magnetic probes.

III. 3-D EMISSION MODEL VALIDATION

To validate the modeling approach, a comparison of modeling results with simulations and measurements has been carried out.

A. Near Field Measurement

To evaluate the EM radiation around the DUT, 3-D near-field measurement is performed. The near-field test bench (see Fig. 3) is constituted of a five-axis robot. It has a mechanical resolution of $10 \mu\text{m}$ in the three directions (x, y, z) and a precision of 0.009° for the two available rotations R_1, R_2 . The maximum scanning area is about $\{200 \text{ cm}(x), 100 \text{ cm}(y), 60 \text{ cm}(z)\}$. The measurement probe is mounted on the robot arm. A system, controlled by a personal computer (PC), is used to monitor the probe displacement in a predefined plane marked by three reference points. Different probes are used referring to the EM field component to be measured. In fact, to measure the tangential component of magnetic field H_x, H_y for the XY plane, two small round loops of a radius equal to 1.6 mm are used. The orientation of the loops according to (x, y) axis determines the component to be measured H_x, H_y . The same loops, but 90° curved, are used to get the normal component of magnetic field H_z .

In 3-D near-field measurement configuration, all the previously cited probes should be placed perpendicular to the plane for which the magnetic radiation should be measured in order to sense the desired component of the magnetic field. A low noise amplifier (LNA) can be inserted into the measurement set-up in order to improve the signal-to-noise ratio (SNR). The two ports (P_1, P_2) of the measurement equipment (network analyzer) are connected respectively to the DUT to inject power for excitation and to the output of the probe to measure the complex transmission parameters S_{21} (magnitude and phase) which will be stored in the PC via GPIB connection. The measured voltage V_m at the probe terminal can then be computed.

In order to get the radiated field, a calibration must be accomplished to obtain the probe antenna factor AF_{probe} so that

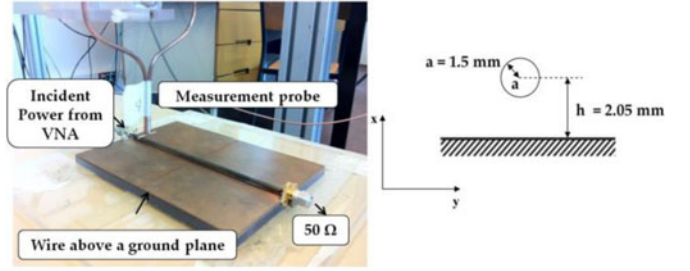


Fig. 4. Calibration setup and Geometrical parameters of the standard circuit.

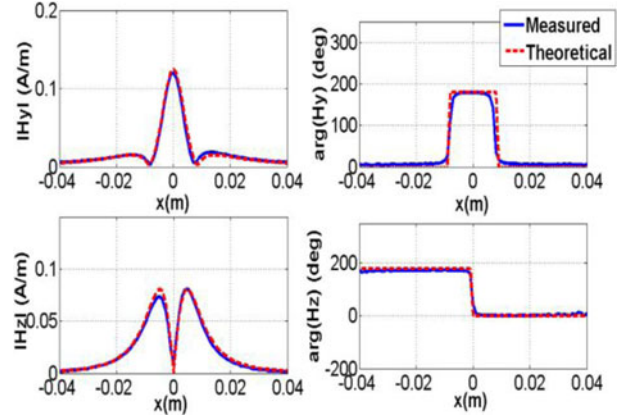


Fig. 5. Comparison between measured and theoretical fields at 5 mm above the wire at $f = 30 \text{ MHz}$.

the complex measured field H_m can be deduced according to V_m . For this purpose, the radiated field of a standard circuit (a conducting wire above a ground plane) is measured H_m and theoretically calculated H_{th} , at the same height and at the frequency of 30 MHz, for both tangential and normal magnetic probes (see Fig. 4). Accordingly, the probe antenna factor can then be calculated ($\text{AF}_{\text{probe}} = H_{th}/V_m$) using the measured voltage at a chosen distance of 3 mm above the wire and theoretical radiated field at the same distance [17].

For validation purposes, the antenna factors are multiplied by the measured voltages at higher distance (5 mm) above the wire to get the radiated magnetic field at this height. Fig. 5 shows a comparison between the measured tangential and normal EM field (magnitude and phase) at 5 mm and their associated theoretical values. The results show that magnetic probes preserve the profiles and good agreement between measured and theoretical fields can be underlined.

The calibration of electric probes is still under investigation [19]. Thus, the electric field solutions of numerical simulations (HFSS-Ansys) are used to validate the 3-D emission model.

B. Validation of the 3-D Emission Model on an “Arch” Device

To validate the modeling approach, we have studied the radiation of a passive 3-D structure: a small “arch” above a ground plane (see Fig. 6). The DUT is simulated in HFSS-Ansys at the frequency of 30 MHz. Thus, a model is built using simulated EM field cartographies on the five faces of a parallelepiped surrounding the DUT $40 \text{ mm}(x) \times 40 \text{ mm}(y) \times 14 \text{ mm}(z)$ (V2). A

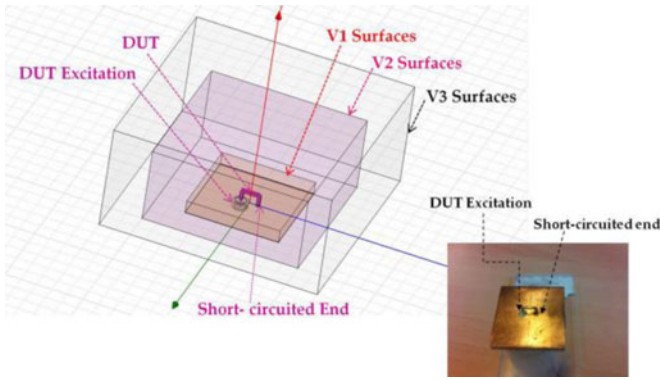


Fig. 6. DUT, a small “arch” above a ground plane: perturbing circuit.

TABLE I
ERRORS BETWEEN SIMULATION AND MODELING ON V2 SURFACES

	XY	XZ2	YZ3	XZ4	YZ5
E_x	0.39	1.21	1.34	0.07	1.34
E_y	0.45	3.11	0.69	1.29	0.67
E_z	0.54	0.02	0.09	0.09	0.08
H_x	0.53	1	0.03	1.13	0.03
H_y	0.46	0.11	0.1	0.09	0.09
H_z	0.48	0.69	0.61	1.25	0.52

set of 260 elemental electric dipoles and 260 magnetic dipoles, distributed on the five surfaces of a $30 \text{ mm}(x) \times 30 \text{ mm}(y) \times 4 \text{ mm}(z)$ volume (V1), has been used to build up the model.

The dipoles number is adjusted by the user basing on the error formulation [see (5)] (see [5] and [6]); we have decided to consider an error which does not exceed 4% in all of the five surfaces of the validation volume V2.

Table I resumes all the error percentages in the different surfaces of V2

$$\text{error}(\%) = \sum_{i=1}^M \left(\frac{|(H/E)_{\text{sim}}(M_i) - (H/E)_{\text{mod}}(M_i)|^2}{\sum_{i=1}^M |(H/E)_{\text{sim}}(M_i)|^2} \right) 100. \quad (5)$$

First, the model has been validated on the volume used to construct it (V2). A 3-D-near field measurement is carried out to collect magnetic fields on the five surfaces of V2. Fig. 7 presents the results of modeled, simulated, and measured magnetic field in V2. Modeled results appoint equivalent sources radiated field, simulated results are deriving from the EM simulation under HFSS-Ansys and measured results are data collected from the near-field measurement.

Cross sections in some arbitrary chosen planes are represented in order to compare results in a more clear way. Fig. 8 presents a comparison between modeled, simulated and measured magnetic fields in cross sections taken in XY and XZ planes. A good agreement between modeled and simulated magnetic field in the different planes can be highlighted. The difference between modeled and measured results can be explained by the fact that the 3-D emission model is built referring to simulated EM field

cartographies, not to measured components. Moreover, the lag between simulated and measured cross sections can be explained by the probe positioning error. In fact, this operation is manually done and it becomes more fastidious to gain a very high probe position's precision with respect to the DUT mainly in a 3-D space. However, the obtained results allow us to validate both the 3-D near-field measurement technique and the 3-D emission model of the DUT. A second model validation, with comparison to simulated results, has been carried out on another volume V3: $50 \text{ mm}(x) \times 50 \text{ mm}(y) \times 24 \text{ mm}(z)$. Fig. 9 presents the obtained results. The errors between modeled and simulated fields are evaluated referring to cross sections arbitrarily chosen in some planes (see Fig. 10). A very good agreement can be underlined between modeled and simulated fields in the second volume of validation.

IV. STUDY OF COUPLING BETWEEN THE 3-D EMISSION MODEL AND A TRANSMISSION LINE

In novel electronic boards, interconnected devices are mounted adjacent to each other in a confined space. However their radiations can cause serious EMI problems. Such emissions induce voltages at the TL terminals where other electronic devices can be connected [20]. To predict coupling phenomena, different numerical methods such as finite difference time domain (FDTD) [21] or the method of moments (MoM) have been used [22]. Nevertheless, these methods are very consuming in terms of computing times and memory requirements.

In order to overcome such limits, we have considered in this study an analytic resolution of the coupling problem. Different formulations have been proposed in the literature to study the field-to-transmission line (TL) coupling [13]–[15]. These analytic solutions have been established from mathematical derivation of the general field-to-TL coupling equations for the case of a round wire above a perfectly conducting ground plane and under the TL theory approximation [23] in order to compute the induced voltages in the TL extremities presented in Fig. 11: a cylindrical conducting wire above a ground plane.

A. Overview on Coupling Formulations

Depending on the exciting field components, three analytic formulations have been adopted to evaluate the induced voltages.

The first model, Taylor model, reported in [13] predicts the coupling on a TL taking into account the action of both exciting electric and magnetic fields. Taylor's approach characterizes the effect of the EM disturbance by both voltage $V_s(y)$ and current $I_s(y)$ sources. $V_s(y)$ and $I_s(y)$ represent, respectively, the influence of the exciting transverse magnetic field H_x and the effect of the vertical electric field E_z distributed along this line. The equivalent circuit model of the TL is presented in Fig. 12; where: L and C are respectively the per-unit-length inductance and capacitance, and the index “e” stands for exciting fields which are the sum of the incident and the ground plane-reflected fields.

BLT (Baum Liu and Tesche) equations [24] have been used, in the frequency domain, to compute the induced voltages on

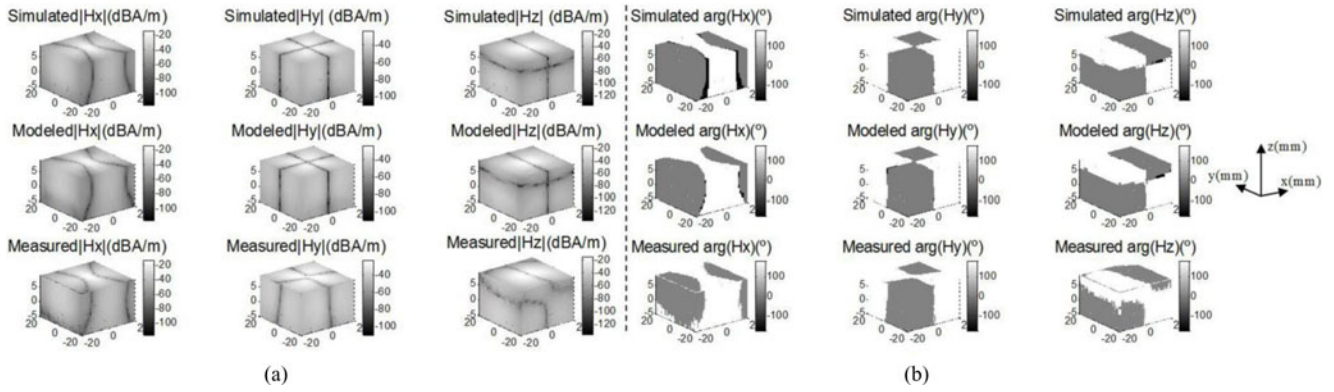


Fig. 7. Simulated, modeled, and measured magnetic field in a volume 40 mm(x) \times 40 mm(y) \times 14 mm(z): (a) Magnitude. (b) Phase.

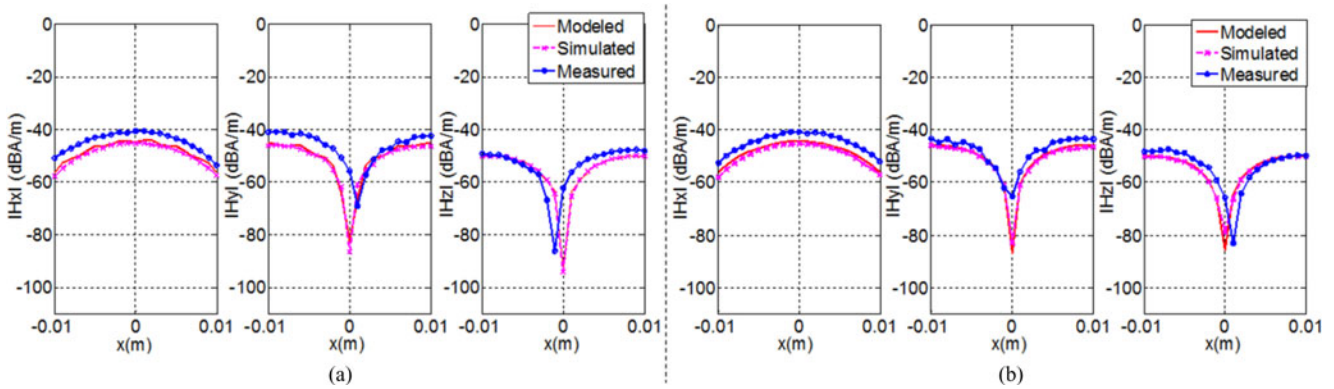


Fig. 8. Comparison between modeled, simulated and measured magnetic field: (a) Cross section in XZ Plane ($y < 0$) at $z = 0$ mm (b) Cross section in XZ Plane ($y > 0$) at $z = 0$ mm.

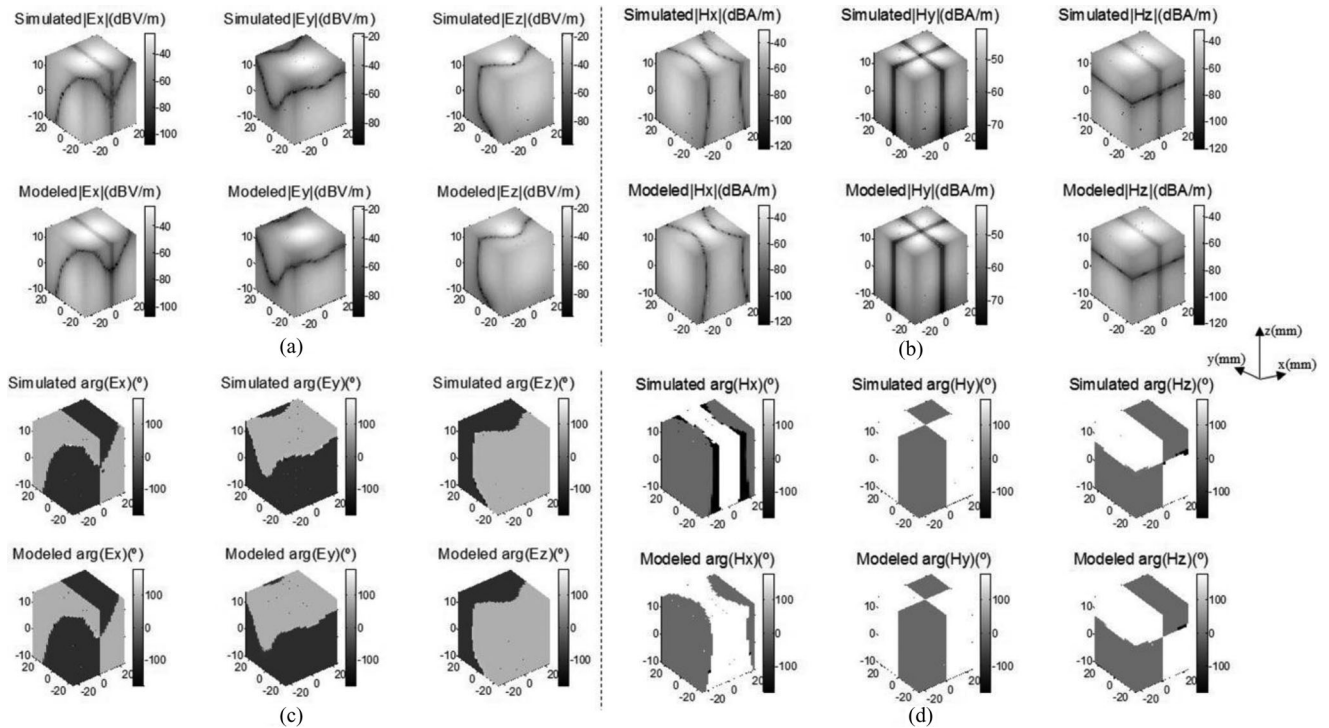


Fig. 9. Simulated and modeled EM field in a volume 50 mm(x) \times 50 mm(y) \times 24 mm(z): (a) Magnitude of electric field. (b) Magnitude of magnetic field. (c) Phase of electric field. (d) Phase of magnetic field.

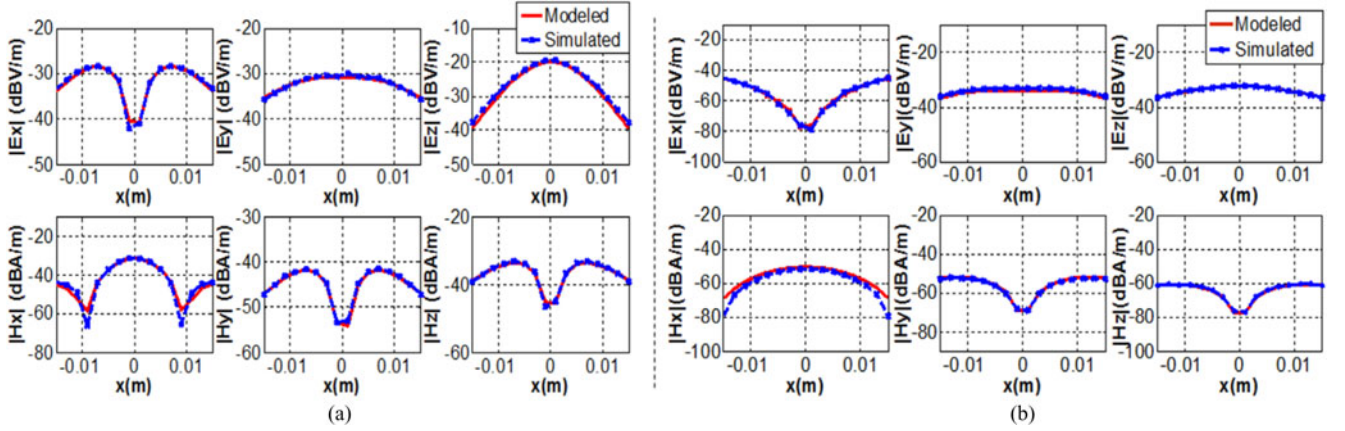


Fig. 10. Comparison between modeled and simulated EM field: (a) Cross section in XY Plane at $y = 5$ mm. (b) Cross section in XZ Plane ($y < 0$) at $z = 0$ mm.

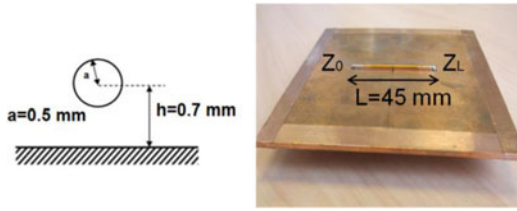


Fig. 11. The transmission line: Victim circuit.

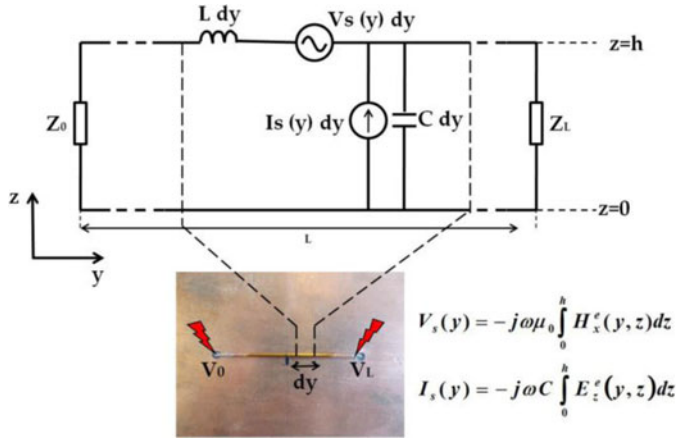


Fig. 12. Equivalent transmission line circuit corresponding to Taylor's model.

the two extremities as presented in the following equation:

$$\begin{bmatrix} V(0) \\ V(L) \end{bmatrix} = \begin{bmatrix} 1 + \rho_1 & 0 \\ 0 & 1 + \rho_2 \end{bmatrix} \begin{bmatrix} -\rho_1 & e^{\gamma L} \\ e^{\gamma L} & -\rho_2 \end{bmatrix}^{-1} \times \begin{bmatrix} \frac{1}{2} \int_0^L e^{\gamma y} (V_S(y) + Z_c I_S(y)) dy \\ -\frac{1}{2} \int_0^L e^{\gamma(L-y)} (V_S(y) + Z_c I_S(y)) dy \end{bmatrix} \quad (6)$$

where Z_c is the TL characteristic impedance, γ is the propagation constant, and (ρ_1, ρ_2) represent the reflection coefficients in the two line extremities in the following equation:

$$\rho_{1,2} = \frac{Z_{0,L} - Z_C}{Z_{0,L} + Z_C}. \quad (7)$$

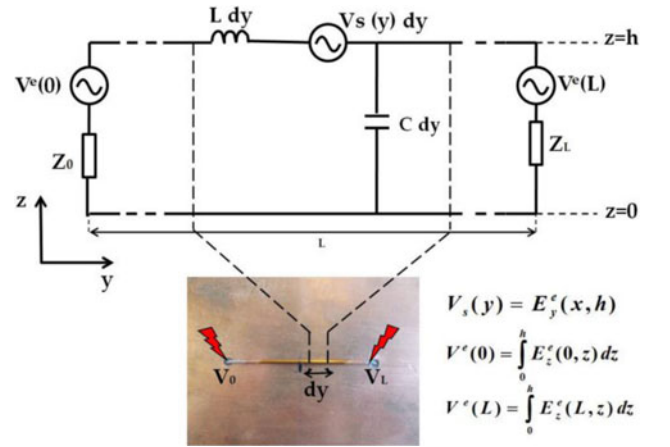


Fig. 13. Equivalent transmission line circuit corresponding to Agrawal's model.

The second coupling model, called Agrawal's model [14] represents the coupling in terms of electric field only. The equivalent TL circuit is presented in Fig. 13.

Agrawal's equivalent model expresses the action of the exciting normal electric field E_z by two voltage sources located in the line extremities: $V_e(0)$ and $V_e(L)$, whereas the effect of the exciting tangential electric field E_y is represented by a distributed voltage $V_s(y)$ along the conducting wire.

For this model, and referring to BLT equations, the induced voltages are expressed in the following equation:

$$\begin{bmatrix} V(0) \\ V(L) \end{bmatrix} = \begin{bmatrix} 1 + \rho_1 & 0 \\ 0 & 1 + \rho_2 \end{bmatrix} \begin{bmatrix} -\rho_1 & e^{\gamma L} \\ e^{\gamma L} & -\rho_2 \end{bmatrix}^{-1} \times \begin{bmatrix} \frac{1}{2} \int_0^L e^{\gamma y} V_S(y) dy - \frac{V^e(0)}{2} + \frac{V^e(L)}{2} e^{\gamma L} \\ -\frac{1}{2} \int_0^L e^{\gamma(L-y)} V_S(y) dy + \frac{V^e(0)}{2} e^{\gamma L} - \frac{V^e(L)}{2} \end{bmatrix}. \quad (8)$$

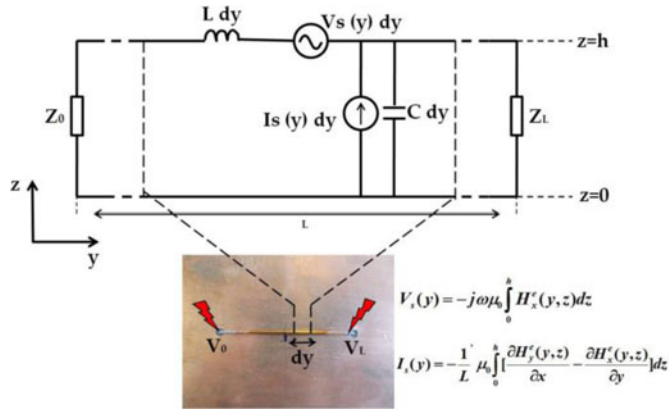


Fig. 14. Equivalent transmission line circuit corresponding to Rachidi's model.

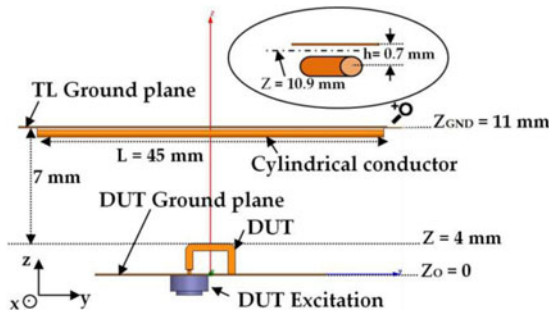


Fig. 15. Setup under study.

The third coupling model explained in [15], called Rachidi's model, presents the field-to-TL coupling in terms of magnetic excitation field. The circuit model is presented in Fig. 14.

For this case, solutions of BLT equations as well as boundary conditions remain unchanged with respect to the case of Taylor's formulation [see (6)].

B. Near-Field Coupling Model

The aim of this study is to predict the coupling between the "arch" (perturbing circuit) and a TL (victim) placed at 7 mm above it as shown in Fig. 15. For this achievement, the perturbing circuit has been replaced by a generic 3-D emission model which does not need any information about physics and design details of DUTs.

For this purpose, in Section III, the DUT is considered as a "black box" which is represented by its 3-D EM radiation model. Thus, the incident EM field can be obtained.

The presence of the TL-ground plane gives rise to reflected fields which can be calculated using the 3-D image theory [18], [25]. Consequently, the excitation field is the sum of the incident and the reflected field computed in the area of interest: a surface delimited by the TL-ground plane and the conducting wire-center (see Fig. 16).

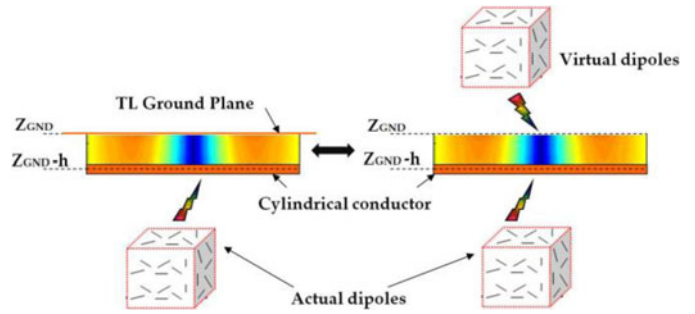


Fig. 16. 3-D Image Theory

In the first step to validate the model, a comparison is carried out between the total EM fields calculated from the radiation of both the 3-D set of dipoles and its image, and the EM simulation results obtained considering the DUT with the presence of the TL ground plane.

Fig. 17 illustrates the comparison between modeled and simulated EM field in a XY plane placed at $z = 10.9$ mm, a height in the area of interest.

Modeled and simulated results have also been compared in an YZ plane, exactly in the area of interest at $x = 10$ mm arbitrarily chosen, as presented in Fig. 18. A good agreement, between modeled and simulated fields can be observed.

These modeled exciting fields associated with the three coupling formulations presented in Section IV-A are implemented in MATLAB [26] to estimate the induced voltages in several positions of the TL along the x -axis and for different configurations of TL load terminals.

To validate our modeling approach, the same setup, including the structure under test and the TL, has been modeled in HFSS-Ansys to compare simulation with model results. A parametric simulation, at a frequency of 30 MHz, has been performed under the same conditions. The obtained results are also validated in practice: the TL was placed above the "arch" in the desired positions and maintained thanks to the robot arm of the near field test bench. Fig. 19 presents the measurement setup.

The movement of the TL along the x -axis is ensured by this robot. A network analyzer is used to excite the DUT and to collect the values of the transmission coefficient S_{21} at the same time. These scattering parameters allow us to compute the values of the induced voltages in the line extremity.

Since the proposed model presents the advantage of taking into account the coupling with both matched and mismatched TL, we have chosen four different scenarios to validate the modeling process:

- 1) $Z_0 = Z_c$: matched TL
- 2) $Z_0 = 0$: short-circuited TL
- 3) $Z_0 = 10 \cdot Z_c$: mismatched TL
- 4) $Z_0 = Z_c/10$: mismatched TL

Obtained results, shown in Fig. 20, with the three coupling formulations (Taylor, Agrawal, and Rachidi) demonstrate the efficiency of the proposed 3-D near field coupling model to predict the induced voltages in different configurations of the wire

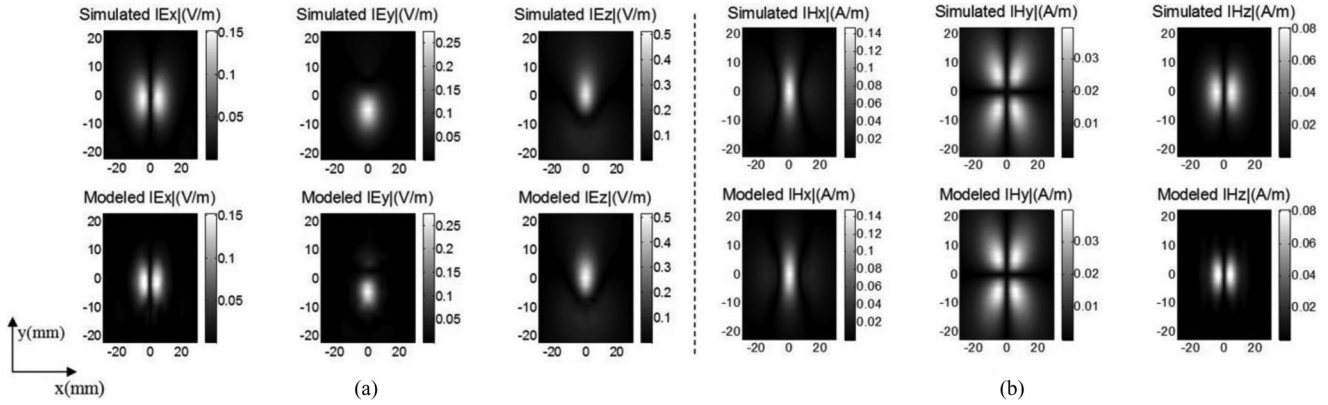


Fig. 17. Comparison between simulated and modeled EM field in XY Plane at $z = 10.9$ mm: (a) Electric field. (b) Magnetic field.

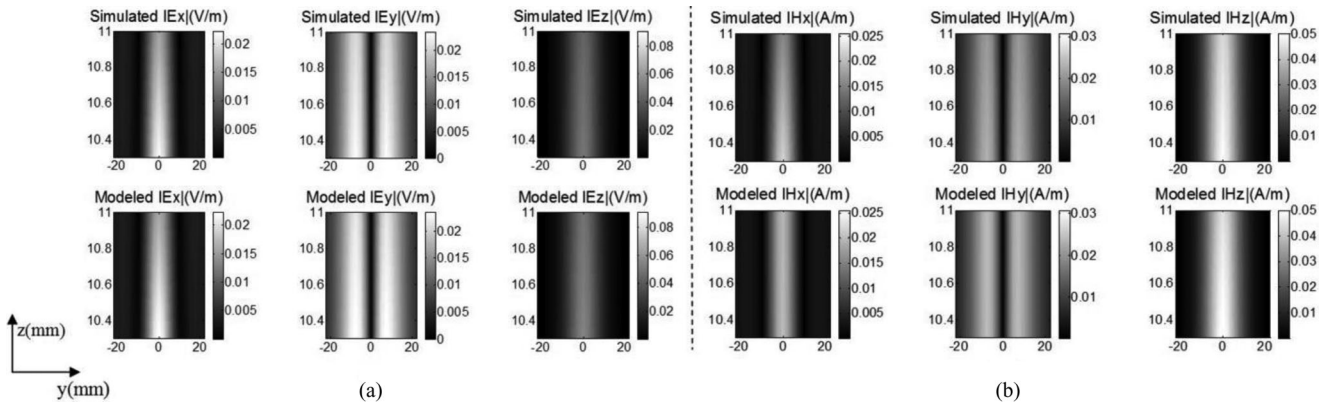


Fig. 18. Comparison between simulated and modeled EM field in YZ Plane at $x = 10$ mm: (a) Electric field. (b) Magnetic field.

victim. The slight difference between measured and modeled results is due to inaccuracies while positioning the line above the DUT since this operation is done manually. These differences become more noticeable when measuring lower levels of induced voltages as in the case of the third configuration ($Z_0 = 10 \cdot Z_c$).

To demonstrate the accuracy of this model, the EM emission of the DUT has been modeled based on a 2-D emission modeling approach. It is necessary to use of 676 electric dipoles and 676 magnetic dipoles, distributed on an X-Y plane, in order to build up and validate the 2-D-emission model [27] basing on the same error formulation expressed in (5). This number of dipoles is largely greater than the 3-D-emission model.

The three coupling formulations have been associated with the 2-D emission model to predict the induced voltages in the line terminals. Two TL configurations have been chosen as illustrative examples to compare results (see Fig. 21) of both 2-D and 3-D models.

The comparison between results of Fig. 20(b) and (a) respectively with results presented in Fig. 21(a) and (b) shows clearly the precision brought by the 3-D near-field coupling model compared with the 2-D approach. For instance, in the

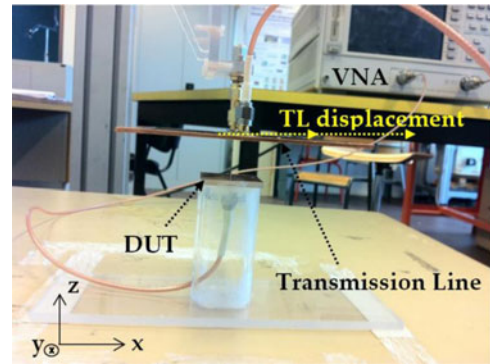


Fig. 19. Measurement setup.

case of matched TL [see Fig. 20(b) and Fig. 21(a)], the model is able to predict the EM coupling (high coupling area $x = 0$ mm is considered) with a relative precision equal to $|\Delta V/V| \sim 2/75 = 2.6\%$ against $|\Delta V/V| \sim 5/75 = 6.6\%$ when considering only the 2-D emission model of the DUT.

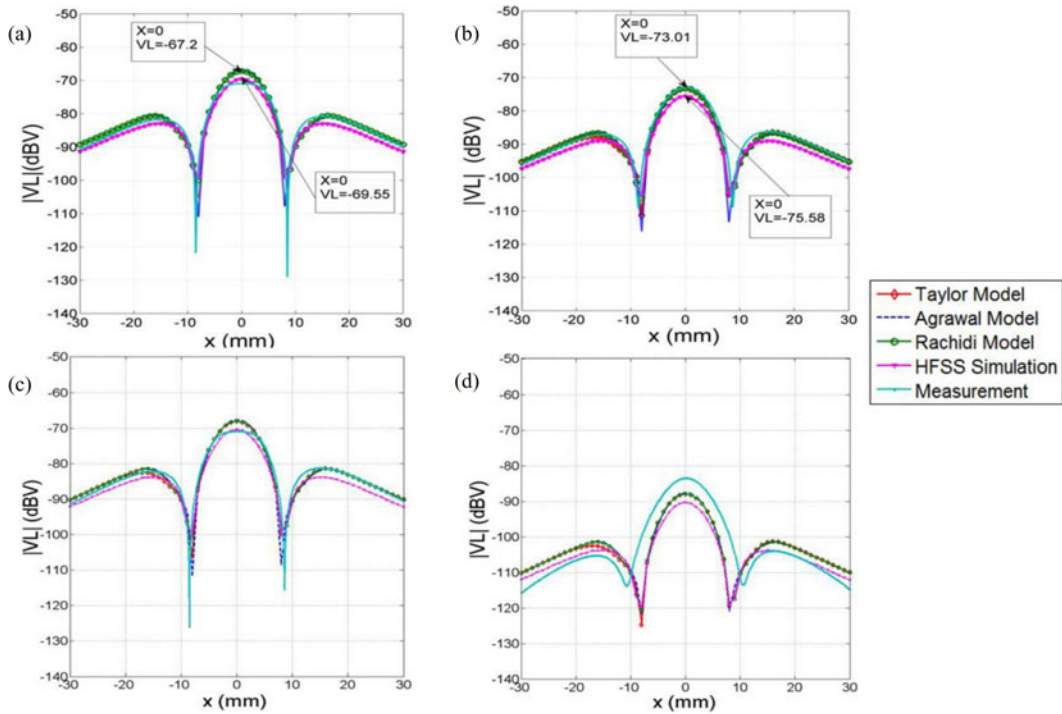


Fig. 20. Induced voltages in different TL configurations-3-D emission model: (a) Short-circuited TL $Z_0 = 0$. (b) Matched TL $Z_0 = Z_c$. (c) Mismatched TL $Z_0 = Z_c/10$. (d) Mismatched TL $Z_0 = 10.Z_c$.

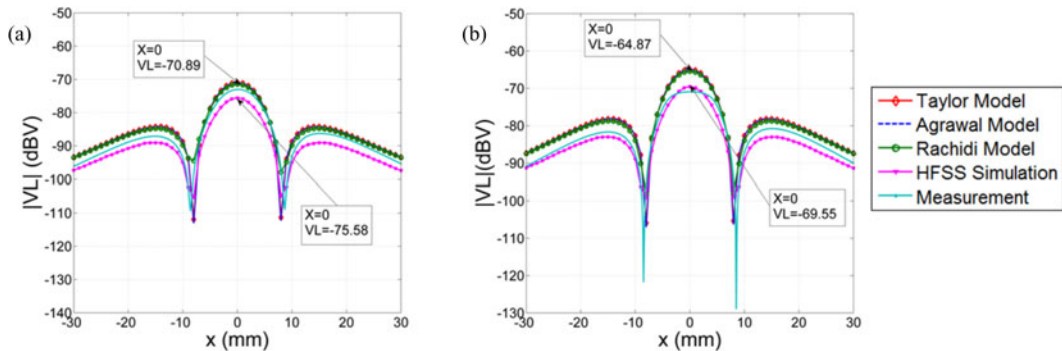


Fig. 21. Induced voltages in different TL configurations-2-D emission model: (a) Matched TL $Z_0 = Z_c$. (b) Short-circuited TL $Z_0 = 0$.

V. CONCLUSION

A simple and accurate coupling model between a perturbing source (“arch”) and a TL (conducting wire above a ground plane) has been presented. The model is based on two concepts: 3-D emission modeling combined with analytic coupling formulations (Taylor, Agrawal, and Rachidi). The 3-D emission model, based on a set of electric and magnetic dipoles distributed on the five surfaces of a well-defined parallelepiped, reproduces the EM radiation in the DUT surrounding space. Tangential cartographies of EM fields are used to build up the 3-D emission model.

The proposed modeling approach presents more accurate results compared with the 2-D near-field coupling models previously developed in anterior works [9]. Furthermore, the 3-D near-field modeling approach requires fewer dipoles. The proposed approach is validated in different TL configurations without any load-matching restrictions. Modeled results are com-

pared with both near-field measurement and EM simulation. The obtained results give information about weak EM coupling regions where components can be properly arranged [28].

These results encourage us to plan further investigations like the coupling between devices and micro strip lines integrated on the same electronic boards. The model can be inserted into EM simulation tools to simplify the prediction of EMI for design engineers.

ACKNOWLEDGMENT

The authors would like to thank the reviewers for their comments to improve the paper readability.

REFERENCES

- [1] L. Beghou, B. Liu, L. Pichon, and F. Costa, “Synthesis of equivalent 3-D models from near field measurements—Application to the EMC of power printed circuit boards,” *IEEE Trans. Magn.*, vol. 45, no. 3, pp. 1650–1653, Mar. 2009.

- [2] A. Taaghoul and T. K. Sarkar, "Near-field to near/far-field transformation for arbitrary near-field geometry utilizing an equivalent magnetic currents," *IEEE Trans. Antenna Propag.*, vol. 38, no. 3, pp. 536–542, Aug. 1996.
- [3] Y. Alvarez, F. Las-Heras, M. R. Pino, and T. K. Sarkar, "An improved super-resolution source reconstitution method," *IEEE Trans. Antenna Propag.*, vol. 58, no. 11, pp. 3855–3866, Nov. 2009.
- [4] P. Li and L. J. Jiang, "The far field transformation for the antenna modeling based on spherical electric field measurements," *Prog. In Electromagn. Res. (PIER)*, vol. 123, pp. 243–261, 2012.
- [5] Y. Vives-Gilabert, C. Arcambal, A. Louis, F. de Daran, P. Eudeline, and B. Mazari, "Modeling magnetic radiations of electronic circuits using near-field scanning method," *IEEE Trans. Electromagn. Compat.*, vol. 49, no. 2, pp. 391–400, May 2007.
- [6] P. F. Lopez, C. Arcambal, D. Baudry, and S. Verdeyme, "Simple electromagnetic modeling procedure: from near-field measurements to commercial electromagnetic simulation tool," *IEEE Trans. Instrum. Meas.*, vol. 59, no. 12, pp. 3111–3121, Dec. 2010.
- [7] A. Ramanujan, Z. Riah, A. Louis, and B. Mazari, "Modeling the electromagnetic radiations of passive microwave components using a near field scanning method," *IEEE Trans. Electromagn. Compat.*, vol. 52, no. 4, pp. 1056–1059, Nov. 2010.
- [8] Z. Yu, J. A. Mix, S. Sajuyigbe, K. P. Slattery, and J. Fan, "An improved dipole-moment model based on near-field scanning for characterizing near-field coupling and far-field radiation from an IC," *IEEE Trans. Electromagn. Compat.*, vol. 55, no. 1, pp. 97–108, Feb. 2013.
- [9] C. Leseigneur, P. F. Lopez, C. Arcambal, D. Baudry, and A. Louis, "Near-field coupling model between electronic systems and a transmission line," in *Proc. IEEE Int. Symp. Electromagn. Compat.*, 2010, pp. 22–27.
- [10] E.-R. Rajkumar, B. Ravelo, M. Bensetti, and P. Fernandez Lopez, "Application of a hybrid model for the susceptibility of complex form metallic wires perturbed by EM near-field radiated by electronic structures," *Prog. Electromagn. Res. B*, vol. 37, pp. 134–169, 2012.
- [11] C. R. Paul, *Introduction to Electromagnetic Compatibility*, 2nd ed. Hoboken, NJ: USA, Wiley, 2006.
- [12] P. Fernandez Lopez, C. Arcambal, and D. Baudry, "3D modeling of radiated emission of electronic components," presented at the 3th Workshop Embedded EMC 2emc, France, Nov. 2010.
- [13] C. D. Taylor, R. S. Satterwhite, and C. W. Harrison, Jr., "The response of a terminated two-wire transmission line excited by a non-uniform electromagnetic field," *IEEE Trans. Antennas Propag.*, vol. 13, no. 6, pp. 987–989, Nov. 1965.
- [14] A. K. Agrawal, H. J. Price, and S. H. Gurbaxani, "Transient response of multiconductor transmission lines excited by a nonuniform electromagnetic field," *IEEE Trans. Electromagn. Compat.*, vol. 22, no. 2, pp. 119–129, May 1980.
- [15] F. Rachidi, "Formulation of the field-to-transmission line coupling equations in terms of magnetic excitation field," *IEEE Trans. Electromagn. Compat.*, vol. 35, no. 3, pp. 404–407, Aug. 1993.
- [16] HFSS from Ansys. (2013). [Online]. Available: <http://www.ansys.com/Products/Simulation+Technology/Electromagnetics/Signal+Integrity+&+Power+Integrity/ANSYS+HFSS>
- [17] D. Baudry, C. Arcambal, A. Louis, B. Mazari, and P. Eudeline, "Applications of the near-field techniques in EMC investigations," *IEEE Trans. Electromagn. Compat.*, vol. 49, no. 3, pp. 485–493, Aug. 2007.
- [18] C. A. Balanis, *Antenna Theory: Analysis and Design*, 2nd ed. New York, USA, Wiley, 1997.
- [19] L. Bouchelouk, Z. Riah, D. Baudry, M. Kadi, A. Louis, and B. Mazari, "Characterization of electromagnetic fields close to microwave devices using electric dipoles probes," *Inter. JRF Microw. Comput.-Aided Eng.*, vol. 18, pp. 146–156, Mar. 2008.
- [20] B. Sreedevi, "EMI issues in UWB systems," in *Proc. 9th Inter. Conf. Electromag. Interf. Compa.*, 2006, pp. 417–424.
- [21] D. M. Sillivan. (2000). "Electromagnetic simulation using the FDTD Method," IEEE Press Series on RF and Microwave Technology, USA. [Online]. Available: <http://www.die.unipd.it/~alotto/download/file2.pdf>
- [22] R. F. Harrington, *Field Computation by Moment Methods*. New York, USA: Macmillan, 1968.
- [23] F. Rachidi, "A review of field-to-transmission line coupling models with special emphasis to lightning-induced voltages on overhead lines," *IEEE Trans. Electromagn. Compat.*, vol. 54, no. 4, pp. 898–911, Aug. 2012.
- [24] F. M. Tesche, "Development and use of the BLT equation in the time domain as applied to a coaxial cable," *IEEE Trans. Electromagn. Compat.*, vol. 49, no. 1, pp. 404–407, Feb. 2007.
- [25] H. Shall, Z. Riah, and M. Kadi, "Prediction of electromagnetic interferences between components and transmission lines," in *Proc. Int. Symp. Electromagn. Compat. EMC EUROPE*, 2012, pp. 1–5.
- [26] MatLab from MathWorks. (2013). [Online]. Available: <http://www.mathworks.fr/products/matlab/>
- [27] H. Shall, L. Laysenne, Z. Riah, and M. Kadi, "3D radiation modeling for a better prediction of the EM coupling between electronic structure and transmission lines," presented at the 16th Int. Colloque on EMC .CEM 2012, France, Apr. 2012.
- [28] H. Shall, Z. Riah, and M. Kadi, "Prediction of 3D-near field coupling between a toroidal inductor and a transmission line," in *Proc. IEEE Int. Symp. Electromagn. Compat.*, 2013.



Hanen Shall (S'13) was born in Sfax, Tunisia, in 1985. She received the Master's Research Degree in Electronics (D.E.A), in 2010, and the Diploma of Electrical Engineering, in 2009, both from the Graduate School of Engineering, University of Sfax, Sfax, Tunisia. She is currently working toward the Ph.D. degree in electronics at the University of Rouen, Mont Saint Aignan, France, and in the Embedded Electronic Systems Research Institute (IRSEEM), Saint Etienne de Rouvray, France.

In November 2009, she joined IRSEEM/Ecole Supérieure d'Ingénieurs, Rouen, France. Her current research interests include electronic components/systems electromagnetic compatibility (EMC), particularly conducted immunity of electronic components: characterization and modeling, near-field measurements for EMC applications, electromagnetic simulations, near-field radiated emission, and immunity modeling of electronic equipment.



Zouheir Riah was born in Constantine, Algeria, on October 16, 1973. He received the Electronic Engineer Diploma from the University of Constantine, Constantine, Algeria, in 1996, and the Master's Research degree (D.E.A) in optoelectronic, optics, and microwave from the National Polytechnic Institute of Grenoble, Grenoble, France, in 2001, and the Ph.D. degree in nonlinear circuits and subsystems from the University of Limoge, Limoges, France, in February 2005.

He completed his Postdoctoral Fellowship at the Research Institute for Embedded Systems (IRSEEM), Rouen, France, in 2008. He is currently a Lecturer at Ecole Supérieure d'Ingénieurs, Graduate Engineering School, Rouen, France, and a Researcher at IRSEEM. His research interests include characterization of electric/magnetic near-field probes, 2-D/3-D near field radiated emission modeling of electronic components, conducted emission modeling of integrated circuits/boards, and EMI modeling techniques.



Moncef Kadi was born in Constantine, Algeria, in March 17, 1974. He received the Diploma in Electrical Engineering from the University of Constantine, Constantine, in 1996, the Master's Research degree (D.E.A) in optoelectronic, optics, and microwaves from the National Polytechnic Institute of Grenoble, Grenoble, France, in 2001, and the Ph.D. degree in RF and Optics from the University Joseph Fourier, Grenoble, in 2004, and the HDR diploma from the University of Rouen, Rouen, France.

In October 2004, he joined the Research Institute for Embedded systems, Ecole Supérieure d'Ingénieurs, Rouen, France, as a Postdoctoral Fellow, and is currently an Associate Professor and the Head of electronic and system research team. His current research interests include the area of electromagnetic compatibility, antennas design, probe characterization, and susceptibility and reliability of electronic components.